U-Band Shield Suspended-Stripline Gunn DRO and VCO

ZHEN-QI HUANG AND QUAN-RANG YANG

Abstract—**A new millimeter-wave IC DRO is proposed. Equations are derived that give the resonant frequency of the DR in suspended stripline (SSL). A *U*-band voltage-controlled oscillator (VCO) with varactor tuning also has been developed. The Gunn diode and varactor used in both of the oscillators are commercially available packaged devices. Restrictions on the performance of the oscillators imposed by packaged and mounted networks and the self-characteristic of the solid-state devices have been analyzed. An electronic tuning range greater than 1000 MHz with an output power exceeding 15 dBm across the bandwidth in the 53 GHz region for the SSL VCO has been realized. The SSL DRO with an output power of more than 17 dBm and a mechanical tuning range of 1.5 GHz in the 54 GHz region has been measured.**

I. INTRODUCTION

THE INCREASING interest in the millimeter-wave region has spurred the development of high-performance millimeter-wave IC RF front end devices [1]–[5]. However, an essential circuit component, a millimeter-wave solid-state oscillator constructed by means of integrated technology with acceptable performance for system applications, is still not available. Most millimeter-wave IC receivers reported use external oscillators with metal waveguide cavities. For this reason, attention has been focused on millimeter-wave IC solid-state sources with low phase noise and high frequency stability, and a wide variety of oscillators have been constructed in microstrip [6]–[8], finline [2], dielectric waveguide [9], lumped elements [10], and suspended stripline (SSL) [11]. It is obvious that DRO's represent a promising approach to the necessary sources for use in millimeter-wave systems. So far, however, the millimeter-wave IC DRO's reported in the literature have been fabricated in a microstrip configuration [6]–[8].

This paper reports a new millimeter-wave IC DRO—a SSL DRO. It is well known that SSL is well adapted to short millimeter-wave waves. This configuration offers several advantages over units in microstrip, finline, etc. There are no drawbacks such as difficulty in grounding a soft substrate in microstrip. Several requirements, such as making substrate holes, welding metal leads to the diode's cap, and bonding wires in microstrip and finline, were omitted by simple and reliable surface connections between the diode and the metal strip of the SSL. This arrangement does not harm the thin cap of the diode and facilitates device replacement. Considering the high price and poorer uniformity of millimeter-wave devices, these facts are rather valuable.

In this investigation, the Gunn diode and the varactor used in both the SSL DRO and the SSL VCO are packaged. So far, millimeter-wave IC VCO's for the most part use varactor chips as electronic tuning elements [18]–[20] in order to avoid the degradation in the electronic tuning range caused by parasitics. we have developed a SSL VCO using a conventional commercial packaged varactor for K_u-band VCO's. A tuning range over 1000 MHz was obtained, which is comparable to that of a VCO utilizing a varactor chip. Restrictions on the performance of the oscillators caused by packaged and mounted networks and the characteristics of the solid-state devices have been analyzed. The SSL DRO, operating in the 54 GHz range, the typical frequency of radiometry for meteorological satellite, had a mechanical tuning range of 1.5 GHz with an output power of more than 17 dBm. The SSL VCO operating in the same frequency range, 53 GHz, had a tuning bandwidth in excess of 1 GHz with an output power of more than 15 dBm across the bandwidth. This performance may represent one of the best results for millimeter-wave IC oscillators to date.

II. DIELECTRIC RESONATOR IN SSL

Excellent mathematical treatments of DR coupled with microstrip have been presented by a number of investigators [12]–[14]. This paper presents a method for calculating the resonant frequencies of DR in SSL.

A rectangular high-dielectric-constant resonator ($l_{x3} \times l_{y3} \times l_{z3}$) mounted on dielectric substrate of suspended stripline (SSL) is shown in Fig. 1. All dielectric materials are assumed lossless and the metallic boundaries are perfectly conducting. The electromagnetic field distribution is $TE_{11\delta}$ mode. The $TE_{11\delta}$ mode field components in the ith

Manuscript received April 21, 1988; revised September 6, 1988. This work was supported by the Ministry of Electronics Industry, China.

Z-Q. Huang is with the Nanjing Electronic Devices Research Institute, P.O. Box 1601, Nanjing, People's Republic of China.

Q.-R. Yang is with the Radio Engineering Department, Nanjing Institute of Technology, Nanjing, People's Republic of China.

IEEE Log Number 8824529.

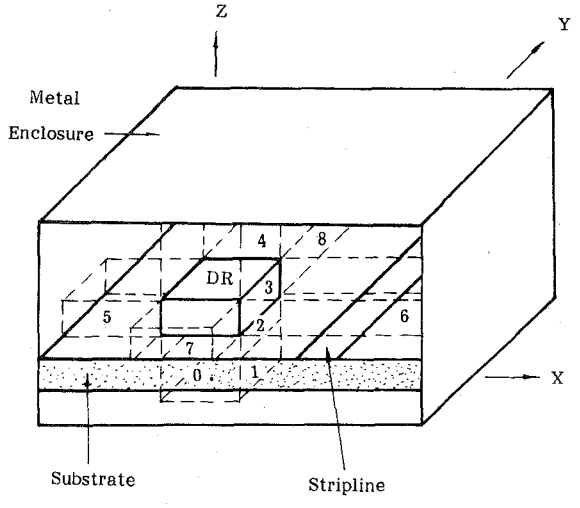

Fig. 1. Dielectric resonator of rectangular cuboid in SSL.

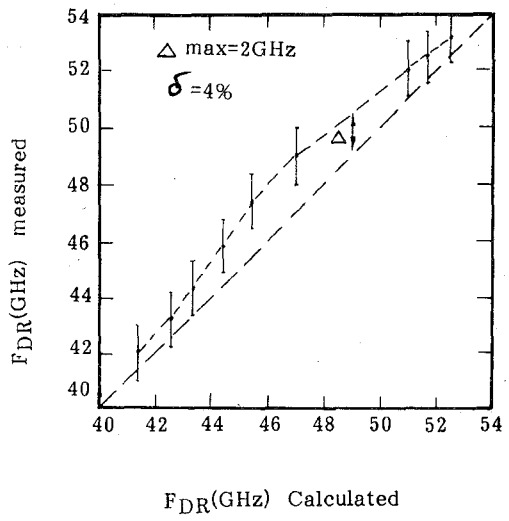

Fig. 2. Comparison of measured and calculated frequencies f_{DR} (GHz) for a set of DR's in SSL.

region can be written as

$$H_z^{(i)} = A_i(x)B_i(y)C_i(z)$$

$$H_x^{(i)} = \frac{1}{k_{xi}^2 + k_{yi}^2} A_i'(x)B_i(y)C_i'(z)$$

$$H_y^{(i)} = \frac{1}{k_{xi}^2 + k_{yi}^2} A_i(x)B_i'(y)C_i'(z)$$

$$E_x^{(i)} = \frac{-j\omega\mu_0}{k_{xi}^2 + K_{yi}^2} A_i(x)B_i'(y)C_i(z)$$

$$E_y^{(i)} = \frac{j\omega\mu_0}{K_{xi}^2 + K_{yi}^2} A_i'(x)B_i(y)C_i(z) \qquad (1)$$

where

$$A_i(x) = A_{1i}shk_{xi}\left(x \pm \frac{l_{x3}}{2}\right) + A_{2i}chk_{xi}\left(x \pm \frac{l_{x3}}{2}\right), \quad i = 5,6$$

$$A_i(x) = A_{1i}\sin k_{xi}x + A_{2i}\cos k_{xi}x, \quad i = 3$$

$$B_i(y) = B_{1i}Shk_{yi}\left(y \pm \frac{l_{y3}}{2}\right) + B_{2i}Chk_{yi}\left(y \pm \frac{l_{y3}}{2}\right), \quad i = 7,8$$

$$B_i(y) = B_{1i}\sin k_{yi}y + B_{2i}\cos k_{yi}y, \quad i = 3$$

$$C_i(z) = C_{1i}Shk_{zi}z + C_{2i}Chk_{zi}z, \quad i = 1,2,4$$

$$C_i(z) = C_{1i}\sin k_{zi}z + C_{2i}\cos k_{zi}z, \quad i = 3. \qquad (2)$$

The wavenumbers (k_{xi}, k_{yi}, and k_{zi}) are related by the wave equation as

$$k_{xi}^2 + K_{yi}^2 = \omega^2\mu_0\epsilon_i \pm k_{zi}^2 \qquad (3)$$

where the minus sign holds for $i = 3$, 5, 6, 7, and 8. The wavenumber of the decaying fields outside dielectric resonators is a real number:

$$(jk_{xi})^2 - k_{yi}^2 = k_{zi}^2 - \omega^2\mu_0\epsilon i, \quad i = 5,6 \qquad (4)$$

$$(jk_{yi})^2 - k_{xi}^2 = k_{zi}^2 - \omega^2\mu_0\epsilon i, \quad i = 7,8. \qquad (5)$$

The relationship between the k_i follows from

$$k_{x1} = k_{x2} = k_{x3} = k_{x4} = k_{x7} = k_{x8}$$
$$k_{y1} = k_{y2} = k_{y3} = k_{y4} = k_{y5} = k_{y6}$$
$$k_{z3} = k_{z5} = k_{z6} = k_{z7} = k_{z8}. \qquad (6)$$

The transcendental equation can be written for the wall admittance matching at the resonator's edge ($x = -l_{x3}/2$, $y = -l_{y3}/2$):

$$\frac{1 - \frac{k_{x3}}{k_{x6}} thk_{x6}l_{x6}\tan k_{x3}l_{x3}}{\frac{1}{k_{x6}}thk_{x6}l_{x6} + \frac{1}{k_{x3}}\tan k_{x3}l_{x3}} - \frac{k_{x5}}{thk_{x5}l_{x5}} = 0 \qquad (7)$$

and

$$\frac{1 - \frac{k_{y3}}{k_{y8}} thk_{y8}l_{y8}\tan k_{y3}l_{y3}}{\frac{1}{k_{y8}}thk_{y8}l_{y8} + \frac{1}{k_{y3}}\tan k_{y3}l_{y3}} - \frac{k_{y7}}{thk_{y7}l_{y7}} = 0. \qquad (8)$$

Another equation can be written for the wall admittance matching at the $z = l_{z1} + l_{z2}$:

$$\frac{1 + \frac{k_{z2}}{k_{z1}} thk_{z1}l_{z1}thk_{z2}l_{z2}}{\frac{1}{k_{z1}}thk_{z1}l_{z1} + \frac{1}{k_{z2}}thk_{z2}l_{z2}} - \frac{1 - \frac{k_{z3}}{k_{z4}} thk_{z4}l_{z4}\tan k_{z3}l_{z3}}{\frac{1}{k_{z4}}thk_{z4}l_{z4} + \frac{1}{k_{z3}}\tan k_{z3}l_{z3}} = 0. \qquad (9)$$

A natural way of solving the system comprising (7), (8), and (9) is to iteratively start with the solution of (7) and (8) using an assumed value of l_{z3} and continue by correcting this value from the solution of (9) and the value of the resonant frequency from (7) and (8). This is an accurate analytical method for computing the resonant frequency of rectangular high-dielectric-constant resonators.

Fig. 2 shows a comparison of the frequencies measured and calculated for a set of DR's. The measured values are

TABLE I
PARAMETERS OF DIELECTRIC RESONATORS

Material	$ZrO_2-SnO_2-TiO_2$	$Ba(Zn_{0.33}Nb_{0.67})O_3-Ba(Zn_{0.33}Ta_{0.67})O_3$
ϵ_r	37.5	29.7
Mode	$TE_{11\delta}$	$TE_{11\delta}$
Q_0 (at 10 GHz)	4300	8000
Dimensions (mm)	$0.98\times0.98\times0.42$	$1.11\times1.11\times0.48$

given over a small frequency region because the position of the frequency tuning post is difficult to determine exactly. However, this theoretical method can be satisfactory for engineering design.

The parameters of the DR's used in the SSL DRO are listed in Table I.

III. SSL DRO

A. DRO Configuration

A schematic of the DRO is shown in Fig. 3. This is a band-reflection-type DR stabilized Gunn oscillator with single tuned behavior. The DR with dummy load was coupled with the SSL in the left side of the Gunn diode to form the band-rejection filter. The output power was fed into WR19 waveguide through a probe (dc block omitted for simplicity) on the right side of the Gunn diode. By using a print technology in order to lower the cost, the circuits were formed on 0.254-mm-thick RT/Duroid 5880 substrate with a relative dielectric constant of 2.22. A packaged Gunn diode was mounted on the lower ground plane of the SSL housing, which also acts as a heat sink. The top electrode of the diode was connected electrically to the metal stripline of the SSL by a simple and reliable surface contact without soldering. Circuits can be fabricated on both sides of the substate. The dc bias network for the Gunn diode and the impedance transforming circuit were placed on the lower side of the circuit board. The DR and related SSL resonant system, coupled by a broadside coupler with a Gunn diode, were arranged on the upper side. Because the DR is "suspended" and is away from "ground," the usual degradation of the Q value was reduced. The distance between the diode and the DR was not limited by their transverse size due to their separation by the substrate. The height of the lower side of the suspended substrate above the bottom of the metal housing, h_2, was designed to be equal to that of the Gunn diode, and a quarter-wavelength matching transformer was used to set the impedance seen by the diode. The height h_1 was made higher than h_2 to provide sufficient space for the DR and its tuning mechanism. The transverse dimensions of the SSL housing must be constrained to cut off the LSM_{11} dominant waveguide mode.

B. Design Considerations

Analyses of Gunn DRO's in MIC's have been reported [15], [16], but the circuit models do not deal with the parasitic effect of the package and mounting of the diode.

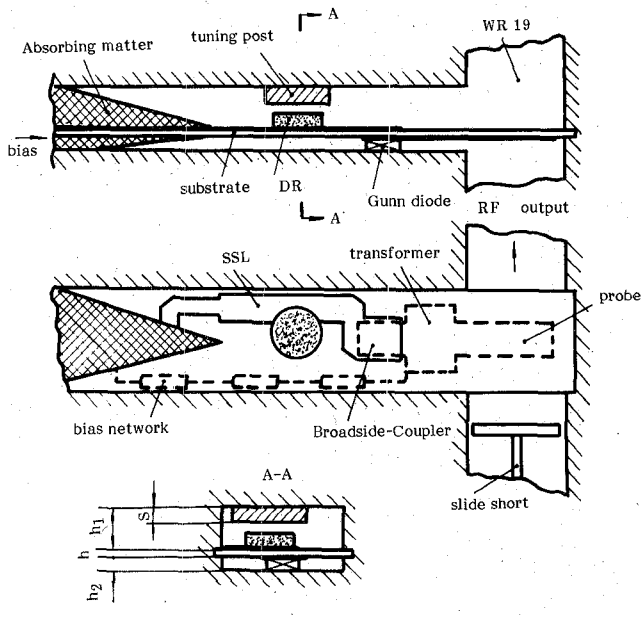

Fig. 3. Schematic of the SSL DRO (low surface dashed lines).

At millimeter-wave frequencies up to U-band, it is necessary to take account of this effect.

Fig. 4 shows the equivalent circuit of the SSL DRO. The symbols used are defined in the figure. A conventional method of analyzing the oscillator circuit is as follows: Choose a reference plane at $D-D'$, find the normalized admittance $\bar{Y}_D(\omega\cdot A)$ of the bare chip seen from $D-D'$ (ω the angular frequency, A the RF voltage amplitude), find the normalized admittance $\bar{Y}_c(\omega)$ of the external circuit seen from $D-D'$, and then solve the following equations by means of numerical iteration [17]:

$$\bar{Y}_D(\omega\cdot A)+\bar{Y}_c(\omega)=0 \tag{10}$$

$$\bar{Y}_D(\omega\cdot A)=+\bar{g}(\omega\cdot A)+j\bar{b}(\omega\cdot A) \tag{11}$$

$$\bar{Y}_c(\omega)=\bar{g}_c(\omega)+j\bar{b}_c(\omega) \tag{12}$$

$$\frac{\dfrac{\partial\bar{b}_c(\omega)}{\partial\bar{g}_c(\omega)}-\dfrac{\partial\bar{b}(\omega\cdot A)}{\partial\bar{g}(\omega\cdot A)}}{\dfrac{\partial\bar{g}(A)}{\partial A}\cdot\dfrac{\partial\bar{g}_c(\omega)}{\partial\omega}}>0. \tag{13}$$

The conventional method mentioned above usually results in a $\bar{Y}_c(\omega)$ that is too complicated. In addition the effect of the diode's embedding network is drowned out by the very complicated $\bar{Y}_c(\omega)$ so that it is not clear how to design the embedding network or order a package with specific parameters.

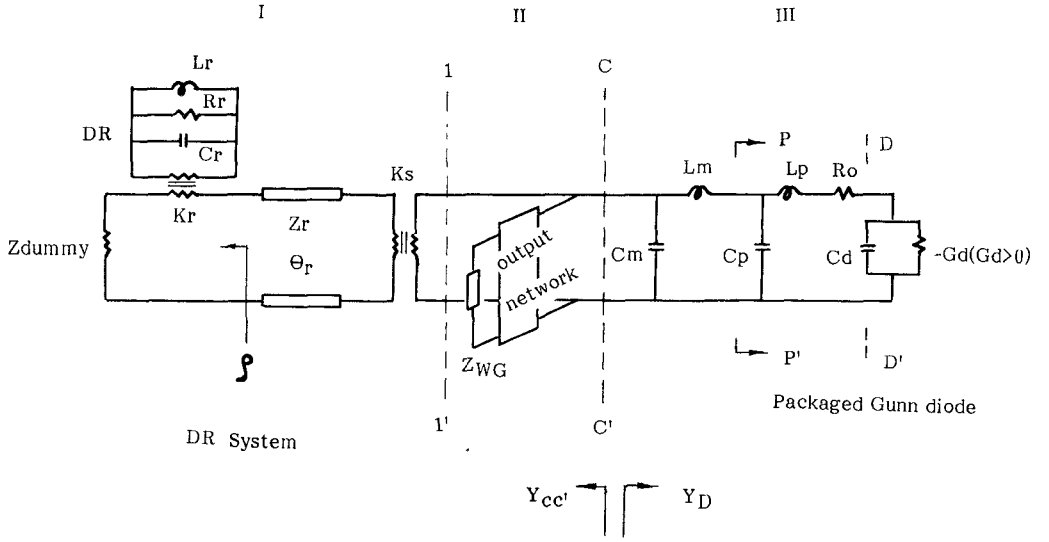

Lm, Cm — mounting parameters of Gunn diode

Ks — Coupling Coefficient of broadside-coupler

Z_{WG} — WR19 Waveguide impedance

Ro — low field resistance

Lp C_p — packaging parameters of Gunn diode

Cd, Gd — chip parameters of Gunn diode

Fig. 4. Equivalent circuit of the SSL DRO.

We take the reference plane at $C-C'$ and divide the entire oscillation system into three parts. Part I is the resonant system, part II the output matching system, and part III the active device system. We first carry out preoptimizations for the three parts and then solve (10)–(13) by numerical iteration. This approach offers a simplified calculation and the physical concept is clear.

The resonant system will be considered first. As known, the frequency stability and FM noise are determined by the slope of the resonant system admittance versus ω [17]. The normalized admittance $\bar{Y}_{DR}$ seen looking left at $1-1'$ in Fig. 4 (assume $K_s=1$) is expressed as

$$\bar{Y}_{DR}=\frac{(1-2Q_0\delta\tan\theta)+j(2Q_0\delta+\rho\tan\theta)}{(\rho-2Q_0\delta\tan\theta)+j(2Q_0\delta+\tan\theta)}$$

$$=\bar{g}_{DR}+j\bar{b}_{DR} \tag{14}$$

where

$$\delta=f/f_0-1$$

$$\theta=2\pi L/\lambda_g$$

$$Q_0=\text{unloaded } Q \text{ of DR}$$

$$\rho=\text{VSWR}.$$

The quantity f_0 is the resonant frequency of the DR, λ_g is the guided wavelength in the SSL, and L is the distance between the $1-1'$ and the DR's center position. L is chosen as so that $L=n\lambda_g/2$. We obtain the slope of resonant system from (14):

$$S_{DRS}=\left.\frac{\partial\bar{b}_{DR}}{\partial f}\right|_{f_0}=\frac{q}{f_0} \tag{15}$$

$$q=\frac{2(\rho-1)}{\rho^2}Q_0 \tag{16}$$

and the loaded Q_L of the resonant system is given by

$$Q_L=\frac{f_0}{2\bar{g}_{DR}}\left.\frac{\partial\bar{b}_{DR}}{\partial_f}\right|_{f_0}=\frac{q}{2\rho}. \tag{17}$$

The frequency–temperature coefficient $S_d(T)$, caused by τ_d, the change in the susceptance of the device chip with temperature, is given by

$$S_d(T)=\frac{1}{q}\frac{\partial\bar{b}_d}{\partial T}=\frac{\tau_d}{q}. \tag{18}$$

The stabilization loss is expressed as [16]

$$L_{(dB)}=6-20lg\left(2-\frac{1}{\rho}\right). \tag{19}$$

The FM noise of the oscillator related to Q_L of the resonant system is given as follows:

$$\left(\frac{N}{C}\right)_{FM\,SSB}=\frac{1}{2Q_L^2}\left(\frac{f_0}{f_m}\right)^2\frac{KT_{eq}B}{C} \tag{20}$$

where N is the noise power, C the carrier power, f_m the

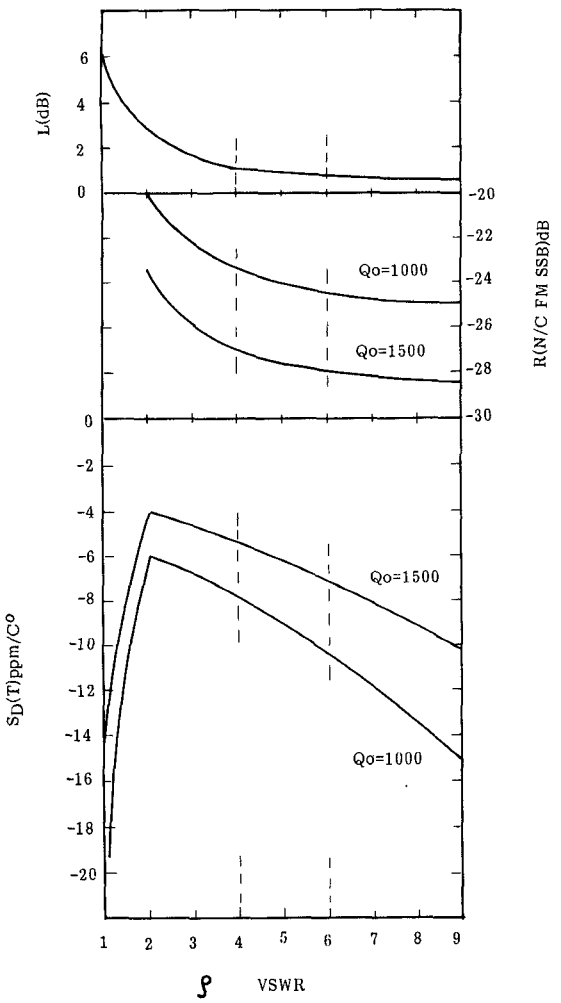

Fig. 5. Relationship between the behavior of the DRO and parameters of the resonant system.

modulation frequency, K the Boltzmann constant, T_{eq} the equivalent noise temperature, and B the bandwidth of noise measured.

Fig. 5 shows the relationships between the parameters mentioned above. In this figure $R(N/C,\text{FM},\text{SSB})$ represents the improved factor of DRO FM noise relative to an oscillator which has the same conditions as that of the DRO except that its Q_L equals only 50. The $S_d(T)$ was evaluated by (18) where $\tau_d = 3\times10^{-3}/°\text{C}$, which is typical for most Gunn devices.

It can be seen from Fig. 5 that in order to stablize $S_d(T)$ and reduce FM noise the unloaded Q_0 of the DR should be as high as possible. However, the VSWR ρ of the resonant system has an optimum region of 4–6. Even though $S_d(T)$ reaches a minimum at $\rho = 2$, we cannot choose $\rho = 2$. If we do, we will lose the output power of 1.5 dB and the FM noise will be degraded 4.1 dB in comparison with $\rho = 5$. At the expense of both output power and phase noise, we just improve the $S_d(T)$ by 4 ppm/°C. By increasing ρ to more than 6, we can obtain an improvement of L (dB) and $R(N/C$ FM SSB) by only 0.5 dB, but the $S_d(T)$ will degrade over 4 ppm/°C. For the reasons given above, the optimum region of the VSWR ρ is 4–6.

Optimization of output system II was aimed at transforming the higher impedance of WR19 standard waveguide to an impedance level matching Y_D and Y_C. In this SSL DRO, the output system consists of a single-section SSL quarter-wavelength immittance transformer, a SSL probe inserted into the E plane of WR19 waveguide, and a WR19 back short. In consideration of narrow bandwidth operation, the SSL probe was designed as a thin stripline which approximates pure inductance. It is easy to tune out the reactance of the probe by using WR19 back short, and the output system becomes a pure resistance R_L. Because of this $\bar{Y}_D$ and $\bar{Y}_C$ are normalized to R_L. Therefore R_L will be optimized automatically in iterative calculations. Then the Z_T, θ_T can be determinated according to R_L.

The optimization of active system III was mainly aimed at the "embedding network." Recently, a model of the Gunn device chip has been improved [10]. Even so, the function $Y_D(A)$ is not yet distinct, but in a narrower region of negative conductance G_d the active capacitance C_d is approximately constant. We can investigate the effect of the embedding network using the values of G_d and C_d. In Fig. 4, the normalized admittance $\bar{Y}_D$ of the packaged Gunn diode seen looking to the right from $p-p'$ is expressed as

$$\bar{Y}_d(\omega\cdot A) = \bar{g}_d(\omega\cdot A) + j\bar{b}_d(\omega\cdot A) \tag{21}$$

$$\bar{g}_d = \frac{\left[(1+q^2)r-1\right](1+q^2)r}{\left[(1+q^2)r-1\right]^2+\left[p+(p-1)q^2\right]^2} \tag{22}$$

$$\bar{b}_d = \omega C_p + \frac{\left[(1+q^2)p-q\right](1+q^2)r}{\left[(1+q^2)r-1\right]^2+\left[p+(p-1)q^2\right]^2} \tag{23}$$

where

$$r = R_0\cdot G_d$$
$$p = \omega L_p\cdot G_d$$
$$q = \omega C_d/G_d.$$

Most V-band packaged Gunn diodes have the following ranges of parameters:

$R_0 = 0.3$–$0.7\ \Omega$ (low field resistance)
$C_p = 0.1$–0.13 pF (packaged capacitance)
$L_p = 0.1$–0.13 nH (packaged inductance, including leads and capsule)
$C_d = 0.09$–0.11 pF (chip capacitance)
$G_d = 20$–40 mS (chip conductance, steady state).

In preoptimization, R_0 can be selected to be 0.5 Ω since $R_0 \ll 1/G_d$. C_p can be measured exactly in static state ($C_p = 0.12$ pF for NSR WT57). L_p will be somewhat different depending on the bonding wires. L_m cannot be avoided, but it is adjustable. L_p together with L_m, which dominates transformation of the active admittance level, will be the main subject of the optimization design.

Fig. 6 shows a numerical iterative example for DRO design. It is well understood from Fig. 6 that once the

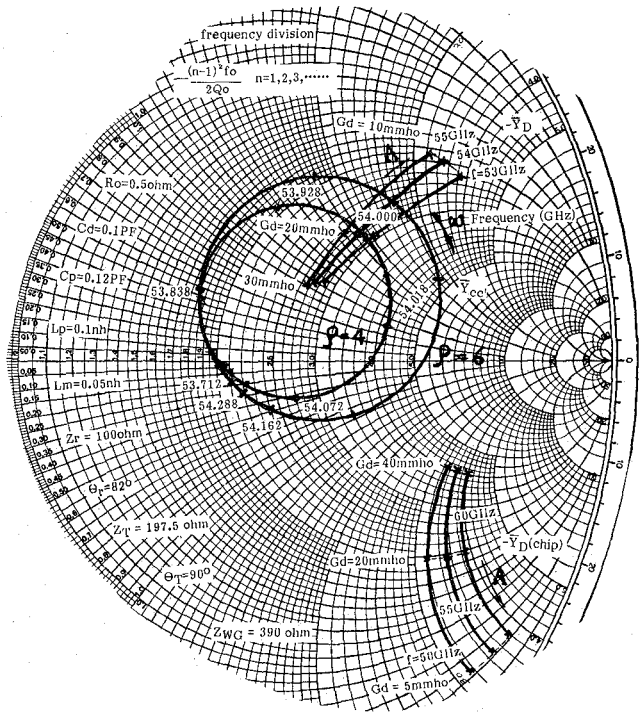

Fig. 6. A graphic example on the Smith chart for DRO design.

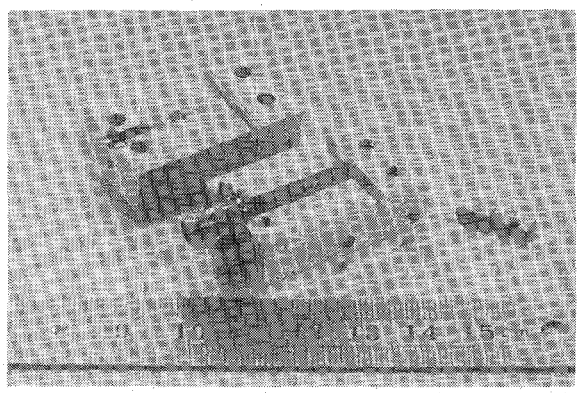

Fig. 7. *U*-band SSL DRO.

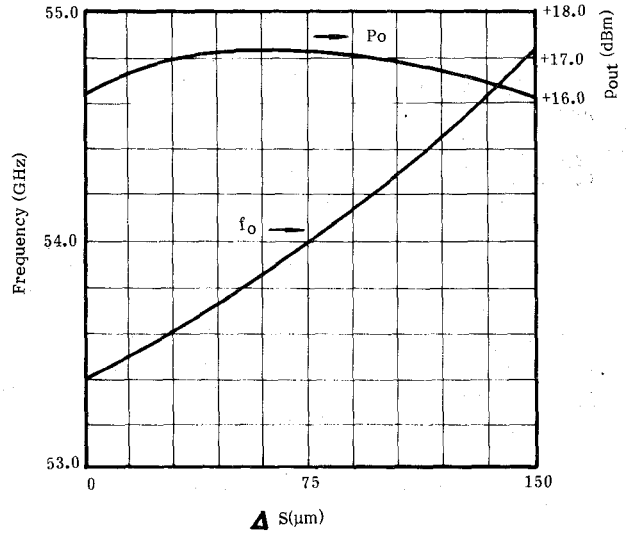

Fig. 8. SSL DRO performance.

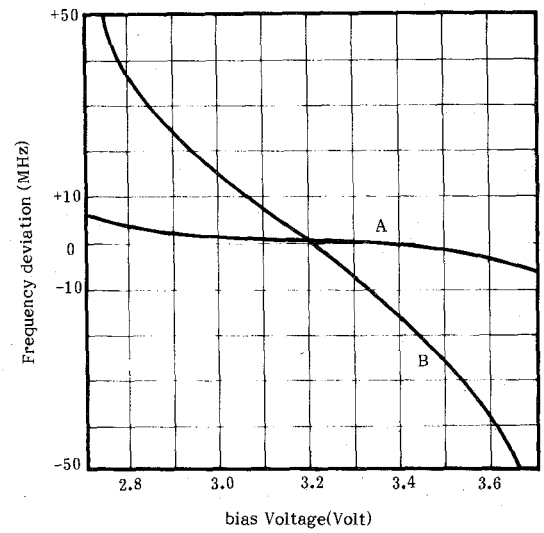

Fig. 9. Frequency-bias characteristics of the SSL DRO.

resonant system has been optimized in accordance with (15)–(20), the design of the packaged and mounting network and θ_T (electrical distance between the Gunn diode and DR) will become the essential factor in realizing the oscillator.

C. Experiment

Fig. 7 shows a photograph of the SSL DRO, and Fig. 8 illustrates the behavior of the DRO with respect to tuning post insertion depth. An output power of more than 17 dB with a mechanical tuning range of 1.5 GHz at 54 GHz has been measured. The oscillating frequency increases linearly with insertion depth s of the tuning post. Note that $df/ds > 0$, which is contrary to $df/ds < 0$ in capacitive load tuning. The tuning slope is in agreement with calculated results, illustrating that the DR functioned as intended. A high and positive slope of 9 GHz/mm allows the τ_f of the oscillator to approach zero by means of double-metal compensation. Fig. 9 shows the bias tuning characteristics of the DRO. Curve (A) represents stabilized performance. Curve (B) shows the behavior without the DR where the DR was replaced by a SSL short and the oscillation frequency was adjusted to the same value as the frequency of the oscillator with the DR. Frequency stability can be inferred from the pushing factor [16]. By comparing A to B, a stabilization factor of 8–10 was achieved.

IV. SSL VCO

A. VCO Configuration

The construction of the SSL VCO, shown in Fig. 10, is similar to that of the SSL DRO. Major differences are as follows: 1) Chebyshev low-pass filters of seven-section high–low impedance, fabricated at the proper positions on the two sides of the substrate, replace the DR system and Gunn diode bias network. 2) A varactor (NSR type WB63 hyperabrupt junction GaAs varactor), acting as an elec-

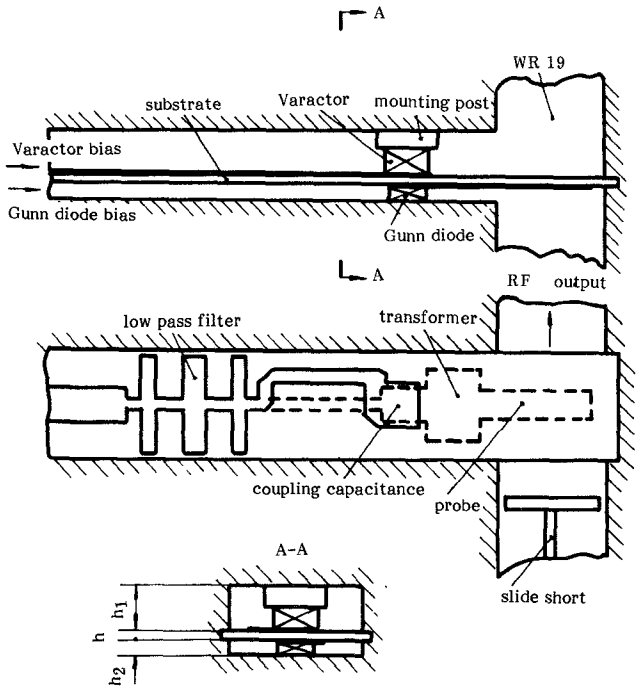

Fig. 10. Construction of the SSL VCO (lower surface dashed lines).

tronic tuning element, was mounted against the Gunn diode in the h_1 "channel." 3) The broadside coupler was replaced by a parallel-plate capacitor which consists of the substrate as dielectric and two metal disk patterns as electrodes on both sides of the substrate.

B. Design Considerations

Fig. 11 describes the equivalent circuit, also divided into three parts. By comparison with the DRO (Fig. 4), parts II and III of the two circuits are the same. The difference is only in the part I. The resonant system for the VCO consists of a coupled capacitance, a short section of SSL, and a packaged varactor and its mounting construction. Emphasis will therefore be placed on analyzing the varactor resonant system.

We first discuss the lossless condition (i.e., $R_s = 0$) and the maximum tuning potential condition (i.e., $\omega C_m - Y_0 \cot \beta L = 0$). For reasons given above, the tuning system impedance Z_s, seen from the left from $E-E'$, is given by

$$Z_s = \omega L_m \frac{\omega^4 - \omega^2(\omega_1^2 + \omega_2^2 + \omega_v^2) + \omega_2^2(\omega_v^2 + m\omega_1^2)}{\omega^4 - \omega^2(\omega_1^2 + \omega_v^2)} \quad (24)$$

where

$$\omega_1^2 = 1/L_v \cdot C_{pv}$$

$$\omega_2^2 = 1/\left[L_{mv} \cdot C_s \cdot C_{pv}/(C_{pv} + C_s)\right]$$

$$\omega_v^2 = 1/L_v \cdot C_j(v)$$

$$m = C_{pv}/(C_{pv} + C_s).$$

In the microwave range, the electronic tuning range was described in terms of the capacitance ratio $\gamma = [C_j(0)/C_{j\min} - 1]$ and the Q factor of the varactor $Q_v = f_{c0}/f_0$ [21]. In our investigation, Q_v became very low ($F_{c0} \cong f_0$) and utilization of γ was also restricted by parasitics.

We discuss the restriction on $C_{j\min}$. If $Z_s = 0$, then a high conductive resonance will be established within the operation frequency range and $\partial B_s/\partial \omega < 0$ will destroy the oscillation conditions (10)–(13). As a consequence, it is necessary to remove this resonance out of band. We derive the low limit of $C_{j\min}$ as follows:

$$C_{j\min}(v) > \frac{25.33}{L_v(nh) \cdot F(\mathrm{GHz}^2)} \quad (25)$$

where

$$F = f_r^2 \frac{1 - (f_1/f_r)^2 - (f_s/f_r)^2/m + (f_1 f_s/f_r^2)^2}{1 - (f_s/f_r)^2/m} \quad (26)$$

$$f_s = 1/2\pi\sqrt{L_{mv}C_s}. \quad (27)$$

L_v, f_1, f_s, and m can be determined according to the embedding network of the varactor chip. Once f_r is obtained, $C_{j\min}(v)$ can be calculated. However, f_r is an unknown quantity, which is related to varactor R_s, load conductance g_L, and active negative conductance $-g_d$, and it is impossible to find the closed solution of f_r in terms of R_s, g_L, and g_d. But we can establish an approximate equation of f_r with the help of the general characteristics of the resonant circuit and consequently can estimate $C_{j\min}(v)$. It was assumed that the resonant system as seen from $E-E'$ when $Z_s = 0$ is a simple R_s-L-C series resonance circuit. The resonant conductance g_v is given by

$$g_v = \frac{Rs}{R_s^2 + \omega^2 L^2\left[1 - (\omega_r^2/\omega^2)\right]^2}$$

$$\omega_r^2 = 1/LC. \quad (28)$$

We can derive f_r from $g_v + g_L < g_d$:

$$f_r = f\sqrt{1 - \sqrt{n-1}/Q_f} \quad (29)$$

$$Q_f = 2\pi f L/R_s \quad (30)$$

$$n = \left[R_s(g_d - g_L)\right]^{-1}. \quad (31)$$

In the above equation, R_s can be taken approximately equal to the varactor's R_s and $L = L_{mv} + L_v$.

Fig. 12 illustrates the above equations graphically by plotting $C_{j\min}(v)$ against f_0 for a range of values of L_{mv}, L_v, and $\Delta G = g_d - g_L$. From this figure we can see that high conductance resonance will be far away from the operating band with increasing L_{mv} and L_v. Conversely, if $L_{mv} = 0$ (i.e., no external tuning), then this type of WB63 varactor cannot act as a tuning element in the 50 GHz frequency range and only a much narrower tuning bandwidth can be obtained at 55 GHz. If L_m is increased sufficiently, the restriction on $C_{j\min}$ will not exist as the situation in Fig. 12, for $L_{mv} = 0.253$ nH, $L_v = 0.2$ nH. However, an increasing L_{mv} will be accompanied by a reduced electronic tuning sensitivity df_0/dC_j, especially in the vicinity of $C_j(0)$.

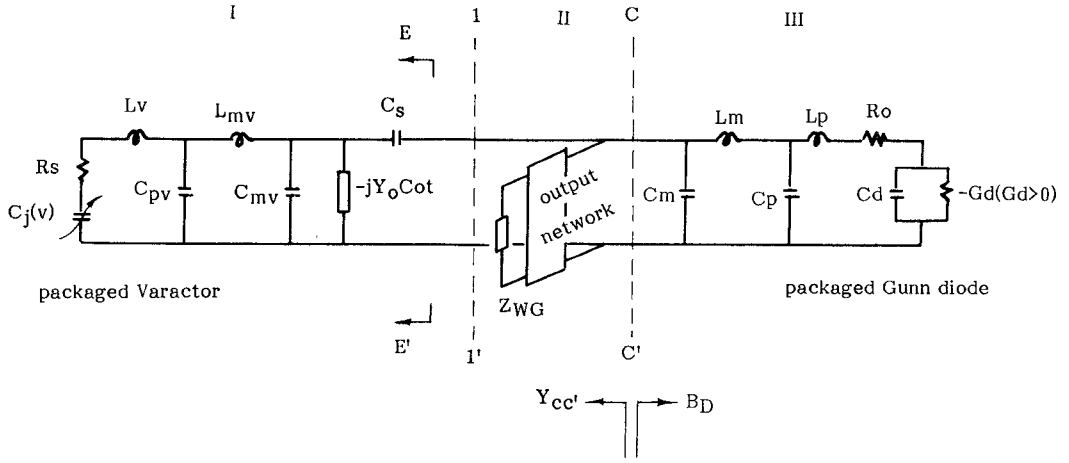

Lmv, Cmv — mounting parameters for varactor

$-jY_0\cot\beta L$ — SSL short section

Cs — coupling capacitance

the other symbols' meaning are the same in Fig. 4.

Fig. 11. Equivalent circuit of the SSL VCO.

The closed resolution of df_0/dC_j does not exist. In order to establish design criteria, we can assume that the susceptance $B(EE')$ seen from the right of $E-E'$ is equal to zero. From this, the resonant frequency was determined by parallel resonance at the $E-E'$ port:

$$\omega^2-\left(\omega_r^2+\omega_1^2\right)=0. \tag{32}$$

From (32), an initial estimate of df_0/dC_j can be found. After that, we can modify the initial value with the help of a numerical method for $B(EE')\neq 0$. This yields an approximate value for the electronic tuning sensitivity:

$$S(C_j)=\frac{\partial f_0}{\partial C_j}=-\frac{0.1625}{C_j\left[L_v\cdot C_j\left(1+C_j/C_{pv}\right)\right]^{\frac{1}{2}}} \quad (\text{GHz}/0.1\text{ pF}) \tag{33}$$

where C_{pv} and C_j are in pF, and L_v is in nH. Fig. 13 shows this equation graphically by plotting $S(C_j)$ versus C_j for several values of L_v. From Fig. 13, it can be seen that $S(C_j)$ decreases sharply with $(C_j)3/2$. Hence it is impossible to compensate for the loss of tuning range resulting from restrictions on $C_{j\min}(v)$ by employing a varactor with higher $C_j(0)$.

From the analyses mentioned above, it can be concluded that

1) The usable range of varactor $C_j(v)$ is restricted by package and mounting parasitics and f_{c0}.
2) To use varactor $C_j(v)$ as effectively as possible, the varactor should have f_{c0} as high as possible, and the design of L_m and C_s should be optimized.
3) Higher negative conductance of the Gunn diode is helpful in effectively utilizing the capacitance ratio; as a result, the tuning bandwidth can be increased.
4) The SSL VCO described in this paper is a millimeter-wave IC VCO with the potential for a wide electronic tuning range in the millimeter-wave frequency range if the following conditions are met:

$$\omega L_{mv}-\frac{1}{\omega C_s}=0 \tag{34}$$

$$\omega C_{mv}-Y_0\cot\beta L=0 \tag{35}$$

$$\left(R_L\cdot g_d\right)^2\gg 1 \tag{36}$$

$$\left(R_L\cdot g_v\right)^2\gg 1. \tag{37}$$

The SSL VCO will become a series tuned type of VCO with broad-band tuning ability (in excess of 6–7 GHz). So for, however, the SSL VCO's reported [11], [22] are all still far short of this prediction. In our calculations and experiments, we have found the reason for this to be the difficulty in satisfying (36) and (37). In addition, the circuit design satisfying (34) and (35) is restricted by mechanical construction, exactness of the circuit models, and fabrication tolerance.

The theoretical tuning range is in agreement with experiment results, illustrated in Fig. 14. The theoretical calculation ended at $C_j(v)=0.15$ pF because $C_{j\min}(v)=0.158$ pF, evaluated according to (25). A wider tuning range, more than 2 GHz, can be expected. The authors have observed a tuning range of 1.7 GHz, with an output power below 10 mW.

C. Experiment

Fig. 15 provides a photograph of the SSL VCO. Experimentally, as shown in Fig. 16, a 1000 MHz tuning range was achieved with an output power exceeding 15 dBm across this electronically tuned bandwidth around 53 GHz. In this investigation, complete integration has been real-

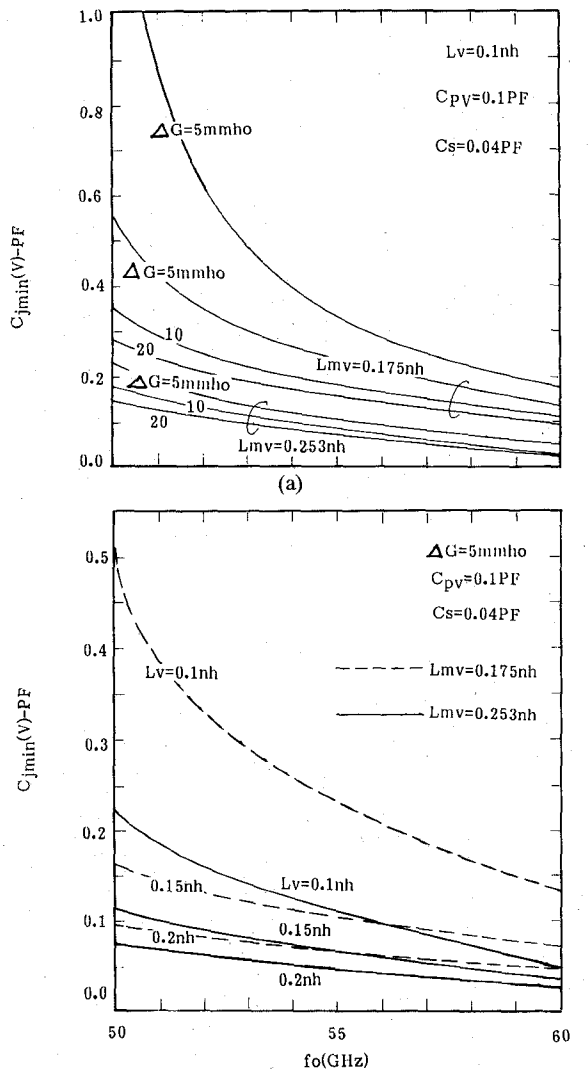

Fig. 12. Dependence of $C_{j\min}(v)$ on frequencies when circuit parameters are varied: (a) effect of L_{mv}, g_d, and g_L on $C_{j\min}(v)$; (b) effect of L_v and L_{mv} on $C_{j\min}(v)$.

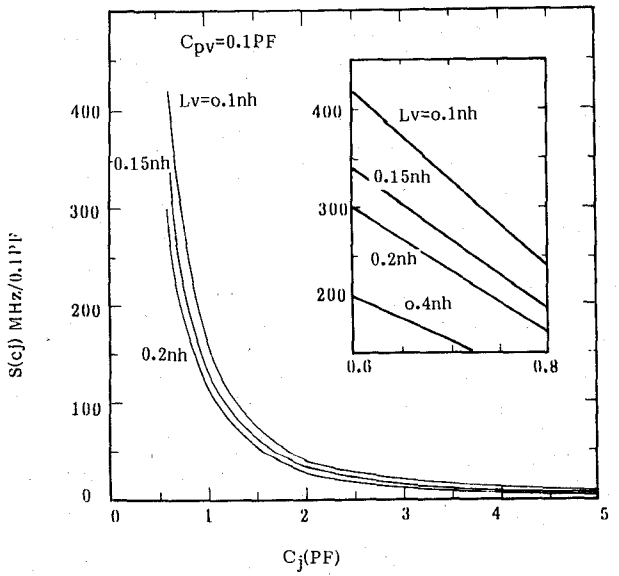

Fig. 13. Electronic tuning sensitivity $S(cj)$ versus C_j in the vicinity of $C_j(0)$ for several values of L_v and C_{pv}.

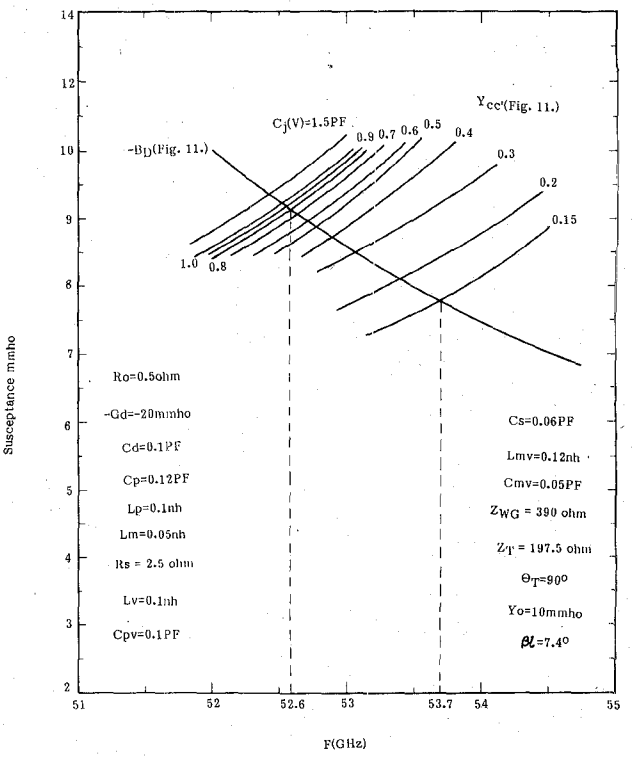

Fig. 14. Theoretical tuning bandwidth in relation to experimental results.

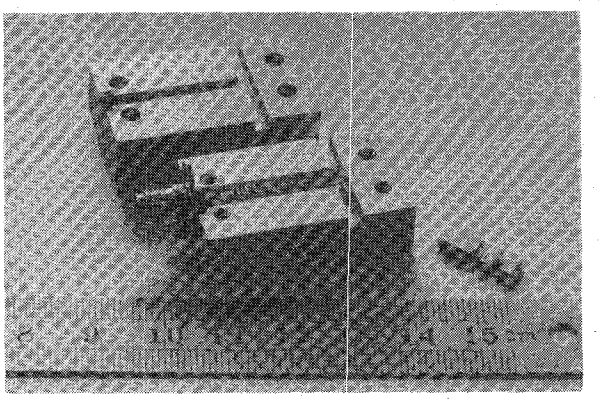

Fig. 15. *U*-band SSL VCO.

ized by comparison with [11], where a sliding short was employed in the SSL channel.

V. Conclusion

A *U*-band SSL DRO and SSL VCO, using packaged devices, have been demonstrated. The performance of these oscillators may be among the best results for millimeter-wave planar hybrid IC solid-state sources to date. The theoretical resonant frequency of the DR in SSL has been verified by measurement. The analysis and design criteria proposed dealing with the embedding networks of the devices and resonant systems have been confirmed by experiments. The authors are confident that the configuration can be made to operate at shorter millimeter wavelengths.

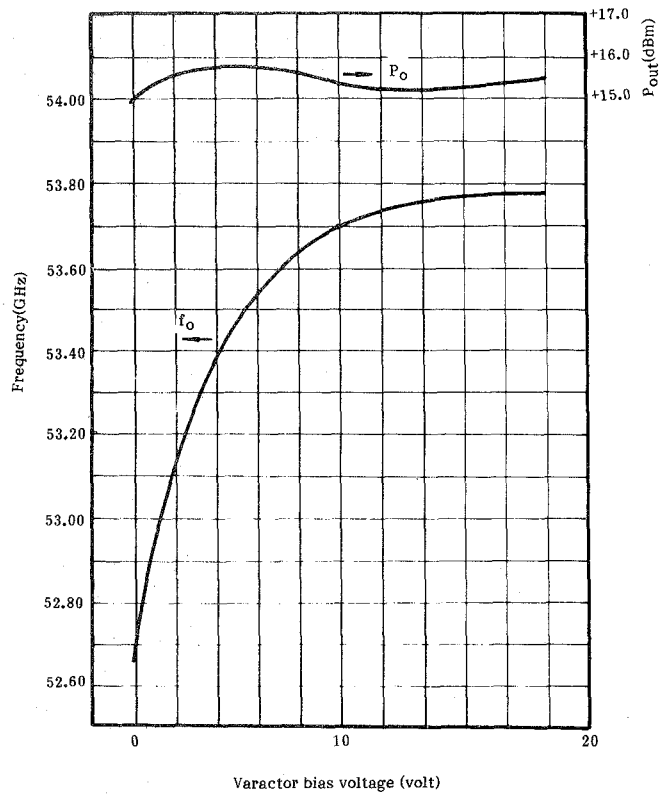

Fig. 16. SSL VCO performance.

References

[1] L. Cohen *et al.*, "Advanced mm-wave receivers for EW applications," *Microwave J.*, vol. 29, no. 4, pp. 127–146, Apr. 1986.

[2] P. J. Meier, "Integrated finline: The second decade—Part II," *Microwave J.*, vol. 28, no. 12, pp. 30–48, Dec. 1985.

[3] K. Chang *et al.*, "W-band (75 to 110 GHz) microstrip components," in *IEEE MTT-S Int. Symp. Dig.*, 1985, pp. 371–374.

[4] T. H. Oxley and C. Burnett, "mm-wave hybrid microstrip technology—Part II," *Microwave J.*, vol. 29, no. 5, pp. 177–185, May 1986.

[5] W. Menzel, H. Callsen, and K. Solbach, "An integrated receiver front end for a 94 GHz dual polarization radar," in *Proc. 13th European Microwave Conf.*, Sept. 1983, pp. 142–147.

[6] A. Grote, R. S. Tahim, and K. Chang, "Miniature millimeter-wave integrated circuit wideband downconverters," in *IEEE MTT-S Int. Microwave Symp. Dig.*, 1985, pp. 159–162.

[7] G. B. Morgan, "Dielectric Resonators for circuits at short millimeter wavelengths," *Microwave J.*, vol. 29, no. 7, pp. 107–115, July 1986.

[8] Y. Tokumitso, M. Ishizaki, M. Iwakuni, and T. Saito, "50 GHz IC components using alumina substrates," *IEEE Trans. Microwave Theory Tech.*, vol. MTT-31, pp. 121–128, Feb. 1983.

[9] R. E. Horn, H. Jacob, and I. Freibergs, "Integrated tunable cavity Gunn oscillator for 60 GHz operation in image line waveguide," *IEEE Trans. Microwave Theory Tech.*, vol. MTT-32, pp. 171–176, Feb. 1984.

[10] L. D. Cohen and E. Sard, "Recent advances in the modeling and performance of millimeter-wave InP, GaAs VCO's and oscillators," in *IEEE MTT-S Int. Symp. Dig.*, 1987, pp. 429–432.

[11] R. S. Tahim, G. Hayashibara, and K. Chang, "High performance mm-wave suspended stripline Gunn VCO," *Electron. Lett.*, vol. 22, no. 20, pp. 1057–1059, Sept. 25, 1986.

[12] T. Itoh and R. S. Rudokas, "New method for computing the resonant frequencies of dielectric resonator," *IEEE Trans. Microwave Theory Tech.*, vol. MTT-25, pp. 52–54, Jan. 1977.

[13] P. Guillon, B. Byzery, and M. Chaubet, "Coupling parameters between a dielectric resonator and a microstripline," *IEEE Trans. Microwave Theory Tech.*, vol. MTT-33, pp. 222–226, Mar. 1985.

[14] D. Kajfez and P. Guillon, *Dielectric Resonators*. Dedham, MA: Artech House, 1986.

[15] T. Makino and A. Hashima, "A highly stabilized MIC Gunn oscillator using a dielectric resonator," *IEEE Trans. Microwave Theory Tech.*, vol. MTT-27, pp. 633–638, July 1979.

[16] N. Imai and K. Yamamoto, "Design consideration for frequency-stabilized MIC IMPATT oscillators in 26 GHz band," *IEEE Trans. Microwave Theory Tech.*, vol. MTT-33, pp. 242–248, Mar. 1985.

[17] K. Kurokawa, "Injection locking of microwave solid-state oscillators," *Proc. IEEE*, vol. 61, pp. 1386–1410, Oct. 1973.

[18] E. J. Denlinger, J. Rosen, E. Mykietyn, and E. C. McDermott, Jr, "Microstrip varactor-tuned millimeter-wave IMPATT diode oscillators," *IEEE Trans. Microwave Theory Tech.*, vol. MTT-23, pp. 953–958, Dec. 1975.

[19] D. Rubin, "Varactor-tuned millimeter-wave MIC oscillator," *IEEE Trans. Microwave Theory Tech.*, vol. MTT-24, pp. 866–867, Nov. 1976.

[20] K. Chang *et al.*, "*V*-band low noise integrated circuit receiver," *IEEE Trans. Microwave Theory Tech.*, vol. MTT-31, pp. 146–153, Feb. 1983.

[21] D. Cawsey, "Wide-range tuning of solid-state microwave oscillators," *IEEE J. Solid-State Circuits*, vol. SC-5, pp. 82–84, Apr. 1970.

[22] Z.-Q. Huang, "*U*-band shield suspended-stripline (SSL) Gunn DRO and VCO," in *IEEE MTT-S Int. Symp. Dig.*, May 1988, pp. 807–810.

Zhen-Qi Huang was born in Tian Jin, China. He graduated from The University of Science and Technology of China, Beijing, China, in 1963, majoring in radioelectronics.

From 1963 to 1965, he worked for the Institute of Electronics, Chinese Academy of Sciences, Beijing, China. His work involved the measurement of high-frequency transistors and transistor amplifiers. From 1966 to 1967, he was with the East-Chinese Semiconductor Research Institute, Chinese Academy of Sciences, Nanjing, China, working on microwave transistor–varactor multipliers. Since 1968, he has been with the Nanjing Solid State Devices Institute (NSR), now the Nanjing Electronic Devices Institute (NEI). From 1968 to 1976, he was engaged in noise-measurement and noise-reduction techniques for IMPATT's and the measurements of IMPATT, Gunn, and LSA devices. He has developed various high-stability Gunn oscillators, Gunn VCO's, and Gunn amplifiers. From 1977 to 1979, he headed the Microwave Solid-State Sources Group. From 1980 to 1986, he served as Vice-Director of MM-Wave Technology Research Lab, which is responsible for developing Gunn, IMPATT, and HEMT devices and corresponding microwave circuit components and subsystems, such as oscillators, injection-locked amplifiers, high-stability phase-locked sources, FET DRO's, FET VCO's, HEMT low-noise amplifiers, and RF front ends. He is presently Senior Engineer responsible for developing millimeter-wave IC active circuits and subsystems.

Mr. Huang received First Prize of National Science and Technology Advanced Award in China in 1985 for contributions to the field of microwave millimeter-wave solid-state sources. He is a member of the Electronics Society of China.

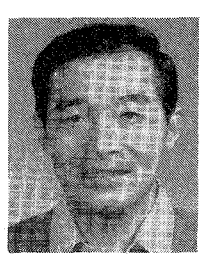

Quan-Rang Yang was born in Jiangsu, China, on September 27, 1934. He graduated from the Nanjing Institute of Technology, Nanjing, China, in 1957.

He is presently a professor in the Department of Radio Engineering at Southeast University, China. He has worked on surface electromagnetic waves since the early 1960's. From 1970 to 1980, he was engaged in research on the theory and design of microwave integrated circuits and numerical problems in electromagnetics. His current research interests include millimeter-wave integrated circuits and dielectric resonators and nonreciprocal devices applied in the millimeter-wave range.

Mr. Yang is a member of the editorial committee of the *Journal of Microwaves* of the Chinese Institute of Electronics.